

## Large Variability in Dominant Scattering from Sentinel-1 SAR in East Antarctica Challenges and Opportunities

Shukla, Shashwat; Wouters, Bert; Picard, Ghislain; Wever, Nander; Izeboud, Maaïke; Husman, Sophie de Roda; Kausch, Thore; Veldhuijsen, Sanne; Matzler, Christian; Lhermitte, Stef

**DOI**

[10.1109/JSTARS.2024.3438233](https://doi.org/10.1109/JSTARS.2024.3438233)

**Publication date**

2024

**Document Version**

Final published version

**Published in**

IEEE Journal of Selected Topics in Applied Earth Observations and Remote Sensing

**Citation (APA)**

Shukla, S., Wouters, B., Picard, G., Wever, N., Izeboud, M., Husman, S. D. R., Kausch, T., Veldhuijsen, S., Matzler, C., & Lhermitte, S. (2024). Large Variability in Dominant Scattering from Sentinel-1 SAR in East Antarctica: Challenges and Opportunities. *IEEE Journal of Selected Topics in Applied Earth Observations and Remote Sensing*, 17, 14380-14393. <https://doi.org/10.1109/JSTARS.2024.3438233>

**Important note**

To cite this publication, please use the final published version (if applicable).  
Please check the document version above.

**Copyright**

Other than for strictly personal use, it is not permitted to download, forward or distribute the text or part of it, without the consent of the author(s) and/or copyright holder(s), unless the work is under an open content license such as Creative Commons.

**Takedown policy**

Please contact us and provide details if you believe this document breaches copyrights.  
We will remove access to the work immediately and investigate your claim.

# Large Variability in Dominant Scattering from Sentinel-1 SAR in East Antarctica: Challenges and Opportunities

Shashwat Shukla, Bert Wouters, Ghislain Picard, Nander Wever, Maaïke Izeboud, Sophie de Roda Husman, Thore Kausch, Sanne Veldhuijsen, Christian Mätzler, and Stef Lhermitte

**Abstract**—Assessing the Surface Mass Balance (SMB) of the Antarctic Ice Sheet is crucial for understanding its response to climate change. Synthetic Aperture Radar observations from Sentinel-1 provide the potential to monitor the variability of SMB processes through changes in the scattering response of near-surface and internal snow layers. However, the interplay between several factors, such as accumulation, wind erosion, deposition, and melt, complicates the interpretation of changes in the scattering of the microwave signal. Additionally, lack of reliable ground truth measurements of the snow surface limits our capability to associate the SMB processes with dominant scattering mechanism. In this study, we aim to quantify the dominant scattering in Sentinel-1 signal and evaluate the changes in scattering in drifting snow-dominated regions of East Antarctica. We introduce a scattering indicator,  $\alpha_{scat,\varepsilon}$ , derived from scattering-type and entropy descriptors. This provides a measure of the dominant scattering between volume and pure scattering. By relating the field measurements to  $\alpha_{scat,\varepsilon}$ , we establish that the evolution of dominant scattering in the presence of snowdrift is complex. First,  $\alpha_{scat,\varepsilon}$  strongly correlates with surface roughness ( $R^2 = 0.92$ ,  $RMSE = 2^\circ$ ). Spatially variable erosion patterns significantly increase the roughness and result in a strong affinity towards pure scattering despite net accumulation. Second, high surface densities also tend to influence pure scattering; however, the effect is dependent on the accumulation rate. With more accumulation, we observe an increasing dominance of volume scattering from internal snow layers. Long-term trends in  $\alpha_{scat,\varepsilon}$  (2017/2023) further suggest that it is challenging to address the causes behind the scattering source based on a single snow surface process. We

thus demonstrate the potential and limitations of  $\alpha_{scat,\varepsilon}$  to infer the variability in dominant scattering from changes in surface processes.

**Index Terms**—Sentinel-1, Scattering, SMB processes, Antarctica.

## I. INTRODUCTION

**S**URFACE mass balance (SMB) is a critical component in evaluating the Antarctic Ice Sheet mass balance and its resulting contribution to global sea level change [1], [2]. SMB includes the sum of surface processes, such as snow accumulation (addition of snow to the firn layer), wind erosion, deposition (accumulations originating from drifting snow, i.e., snow transport by wind in the lowermost 2 m of the atmosphere), sublimation and runoff [1]. Positive SMB occurs when snow accumulation exceeds erosion and runoff of surface meltwater, contributing to ice sheet growth. Negative SMB, where meltwater runoff or sublimation exceeds snow accumulation, contributes to ice loss. However, the properties of near-surface layers are known to be highly spatially and temporally variable, which is challenging to reproduce for regional climate models (e.g., Regional Atmospheric Climate Model; RACMO2) [3] and the SNOWPACK model [4]. This variability is mainly caused by snow accumulation, sublimation, wind-driven deposition, and erosion of snow layers.

One potential way to characterize the local variations of SMB is the use of satellite remote sensing due to its data acquisition capabilities at high spatial and temporal resolution, covering large areas of the ice sheet year-round [5], [6]. This complements field measurements at shorter timescales, which are, in turn, extremely important for evaluating the satellite products. Sentinel-1, a Copernicus Synthetic Aperture Radar (SAR) mission, consists of two polar-orbiting satellites Sentinel-1A and Sentinel-1B, equipped with a phase-preserving C-band dual-polarization (hereafter called dual-pol) system operating at approximately 5.405 GHz [7]. This system transmits a signal in either horizontal (H) or vertical (V) polarization and then receives in both H and V polarizations. The polar orbits of the Sentinel-1 satellites provide a high revisit time over Antarctica. Moreover, the C-band frequency is known for its sensitivity to surface roughness and can penetrate into a snowpack in the order of several meters ( $\sim 15 - 20$  m depth) [8], [9]. Furthermore, the data is acquired at day and night with a frequent revisit time ( $\sim 6$  or 12 days), while the

The work of Shashwat Shukla, Sophie de Roda Husman, and Sanne Veldhuijsen was supported by Nederlandse Organisatie voor Wetenschappelijk Onderzoek (NWO) under grant no. OCENW.GROOT.2019.091. The work of Maaïke Izeboud was supported by the NWO under grant no. ALWGO.2018.043. The work of Thore Kausch was supported by the NWO under grant no. AL-WPT.2016.4. (Corresponding author: Shashwat Shukla.)

Shashwat Shukla, Bert Wouters, Maaïke Izeboud, Sophie de Roda Husman and Thore Kausch are with the Department of Geoscience and Remote Sensing, Delft University of Technology, 2628 CD Delft, The Netherlands (email: s.shukla@tudelft.nl; bert.wouters@tudelft.nl; m.izeboud@tudelft.nl; s.derodahusman@tudelft.nl; T.Kausch@tudelft.nl).

Ghislain Picard is with the Institut des Géosciences de l'Environnement (IGE), Université Grenoble Alpes, 38402 Grenoble, France (e-mail: ghislain.picard@univ-grenoble-alpes.fr).

Sanne Veldhuijsen is with the Institute for Marine and Atmospheric Research Utrecht, Utrecht University, 3584CS Utrecht, The Netherlands (e-mail: s.b.m.veldhuijsen@uu.nl).

Nander Wever is with the WSL Institute for Snow and Avalanche Research SLF, Davos, Switzerland (email: nander.wever@slf.ch).

Christian Mätzler is with the GAMMA Remote Sensing AG, Gümmligen, Switzerland (email: christian.matzler@unibe.ch).

Stef Lhermitte is with the Department of Earth and Environmental Sciences, KU Leuven, 3000 Leuven, Belgium and also with the Department of Geoscience and Remote Sensing, Delft University of Technology, 2628 CD Delft, The Netherlands (e-mail: stef.lhermitte@kuleuven.be).

Manuscript received August 1, 2024

radar is not impacted by cloudiness, the presence of drifting snow, or other weather conditions [8].

When the radar signal interacts with the snowpack, scattering occurs from two primary sources: a) surface layers, where surface roughness controls the radar return (or surface scattering), and b) internal layers, where density variations and individual grains contribute to volume scattering. Field measurements in regions of East Antarctica that are dominated by drifting snow have revealed the formation of erosion/deposition patterns on the surface, exhibiting spatial variations with typical length scales of a few meters [4]. Notably, low-density snow accumulation layers have been observed during periods of low wind conditions, which are subsequently eroded by high wind speed events [4], [10], potentially impacting the roughness. In such a scenario, the dominant signal return to the sensor increasingly stems from the surface layer, with the internal layers contributing less. On the other hand, with snow accumulation, snow height increases and a larger part of the radar signal travels through the snow column [11]. A main reason for this behavior is the changing impedance match at the snow surface. Even a very shallow layer of  $1/4^{th}$  of a wavelength ( $\sim 1$  cm) of soft snow is able to form a nearly perfect impedance match, especially for HH and HV polarization, which eliminates surface scattering and increases volume scattering [12]. Thus, it could be possible to gain qualitative insights to the surface processes such as accumulation or erosion based on volume or surface scattering, respectively. However, quantifying dominant scattering mechanism, between surface and volume, from the radar signal is challenging. In this study, we aim to quantify the dominant scattering from Sentinel-1 as a proxy for changes in snow surface processes in East Antarctica.

Various methods have been developed to determine the dominant scattering based on the analysis of dual-pol SAR data [13], [14], [15]. One reliable technique involves eigen-decomposition of the  $2 \times 2$  covariance matrix derived from dual-pol single-look complex (SLC) data, which enables identification of specific scattering [13]. Here, the average scattering angle is calculated by weighting the two orthogonal polarization states using their corresponding pseudo probabilities, which are also utilized to compute entropy. Ainsworth et al. [15] extended this technique by introducing a scattering-type parameter. However, the processing of SLC data has several limitations: a) it is computationally intensive, time-consuming, and comes with large data volumes as it contains both amplitude and phase information, and b) it has limited interpretability and is less user-friendly due to complex phase information that requires further processing to obtain meaningful information such as coherence or interferometric products. In contrast, Ground Range Detected (GRD) processing addresses the aforementioned limitations by providing calibrated, geo-located, and amplitude-only data, making it more straightforward to interpret and store. Bhogapurapu et al. [16] proposed pseudo scattering-type and entropy parameters within an unsupervised clustering framework applicable for Sentinel-1 GRD data in assessing different stages of crop growth. The approach in itself is qualitative and constrained by the discrete scattering classes, from low entropy pure scat-

tering to high entropy volume scattering [16]. Here, the pure scattering term can be used analogous to surface scattering, as it determines the response from deterministic surface targets [16].

Based on the work of Bhogapurapu et al. [16], we introduce a new quantitative parameter derived from Sentinel-1 GRD data that includes the pseudo scattering-type and entropy information while differentiating the pure scattering from volume scattering. To support our observational findings, we utilize the repeated in-situ measurements of snow surface acquired during the Mass2Ant 2018-2019 and 2021-2022 field campaigns at Hammarryggen and Lokeryggen ice rises in the Dronning Maud Land region, specifically focusing on surface conditions under wind and precipitation events. The goal of this study is twofold: a) to understand how snow surface processes relate to the changes in the dominant scattering from Sentinel-1 signal at the field-scale, and b) to examine the long-term variations in scattering and interpreting the physical processes driving the scattering response of study sites. For the first goal, we derived the surface roughness from field data and used the in-situ snow height calculations from Wever et al. [4] to relate this with surface and volume scattering, respectively. We then computed their respective changes in specified periods during the field campaign and evaluated them against the changes in our proposed Sentinel-1 parameter. For the second goal, we looked at the long-term changes (2017/2023) in the proposed parameter and compared them with the data products of the regional climate model, RACMO2 (for snowdrift erosion and snowfall), and firn model, IMAU-FDM (for surface density). In this way, we are able to investigate the extent to which surface processes can explain the variability in dominant scattering from Sentinel-1.

## II. STUDY AREA AND DATA

### A. Field sites

Our study focuses on two sites near the Belgian research station Princess Elisabeth Antarctica within the Dronning Maud Land region of East Antarctica (Fig. 1). Here, we have extensive in-situ measurements acquired during Mass2Ant field campaigns. This includes detailed snow surface measurements, such as surface roughness, snow height, and surface density, augmented with information on the surface mass balance [4]. The first study site, Hammarryggen (HAM) ice rise, is located at  $70.502^\circ$  S,  $21.874^\circ$  E, approximately 360 m above sea level, where a field campaign was conducted in 2018/19. The second study site is situated on the Lokeryggen (LIR) ice rise, located at  $70.536^\circ$  S,  $24.070^\circ$  E,  $\sim 350$  m above sea level, where a field campaign was executed in 2021/22. LIR borders the Roi Baudouin Ice Shelf from the east, and the site is located in the accumulation zone. Both HAM and LIR are located in the confluence zone and is subjected to frequent drifting and blowing snow (i.e., snow transport by wind in the above 2 m of the atmosphere) along with high wind speeds [17], [18], [19]. Consequently, spatially variable erosion/deposition patterns emerge in these areas. We thus explicitly exploit the field measurements of near-surface layers as a way to understand the changes in the dominant scattering from Sentinel-1.

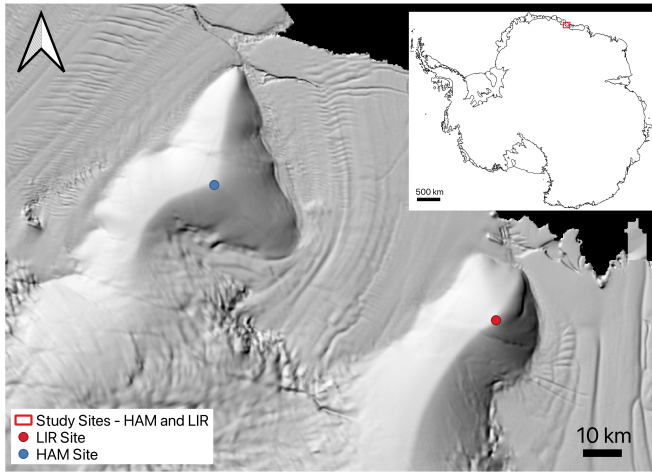


Fig. 1. Study sites on Hammarryggen (HAM) and Lokeryggen (LIR) ice rises marked over the hillshade of the Reference Elevation Model of Antarctica (REMA) of the Roi Baudouin Ice Shelf, Dronning Maud Land, East Antarctica. The red box in the base map of Antarctica represents the study site location.

### B. In-situ roughness measurements

The spatial and temporal variations in snow surface roughness at the HAM and LIR sites were determined through repeated terrestrial laser scanner (TLS) scans. TLS provides a relatively robust method for the derivation of roughness products from the surface scans and serves as a reliable alternative to traditional methods like profilometer, which are typically labor-intensive and prone to misinterpretation [20], [21], [22]. The TLS acquisitions were conducted on multiple days (i.e., 4 days for the HAM site and 2 days for the LIR site), thereby employing a unique field setup to capture the changes in surface roughness and snow height as a consequence of wind and precipitation events.

During the acquisition phase, the maximum effective range of the scanner was limited to  $\sim 250$  m. The azimuth angles covered during scanning encompassed a range of about  $230^\circ$ , corresponding to a scanned area of  $\sim 125,000$  m<sup>2</sup>. We used four reflectors that were installed on bamboo poles as reference points for each scan. The scans were registered with respect to the reflectors in such a way that the successive scans show the spatial patterns of erosion and deposition of snow. Moreover, multiple scan positions were used to create one combined point cloud. The registration of multiple point clouds was accomplished using Leica Cyclone software [23]. To eliminate the effects of tilt and slope of the surface on the roughness calculation, a detrending process was applied by fitting a plane to the registered point cloud data. This also ensured more accurate comparison between scans from different dates. Ultimately, a 3D surface of  $\sim 200 \times 200$  m<sup>2</sup> was generated by rasterizing the detrended point cloud at a spatial resolution of 1 mm, which was necessary to characterize small-scale roughness features sensitive to SAR wavelengths.

At the HAM site, four scans were performed using a Riegl VZ-6000 TLS on 27 Dec 2018, and on 2, 4, and 11 Jan 2019, respectively. The VZ-6000 operates in the infrared region with a wavelength of 1064 nm and an angular measurement

resolution over  $0.0005^\circ$  [24]. Further details on the scan acquisition process and accuracy at the HAM site can be found in Wever et al. [4]. At the LIR site, a 3D surface topography was obtained using a Leica P40 ScanStation operating at a wavelength of 1550 nm, which is suitable for surface roughness measurements of snow due to its limited penetration of less than few a millimeters into the snowpack [25]. Two scans were conducted on 25 Dec 2021 and 5 Jan 2022.

During the fieldwork, we observed melt-freeze crusts near the surface due to warm weather during the days before the actual scan day [4]. At the HAM site, the air temperature reached up to 271 K with distinguishable melt features on Dec 27, and the surface also experienced a limited amount of melt in the period Jan 2 – Jan 4. At the LIR site, the surface exhibited similar melt-freeze crusts on Dec 25, whereas the surface was very smooth with soft snow on Jan 5. Two days before the first scan, i.e., on Dec 23, patches of wet snow indicating moderate melt were observed in the vicinity of the scan location. Weather conditions during the scan days for both sites were mostly characterized by cloud cover, overcast skies, and low wind speeds. The minimum temperature during the acquisition period remained above the minimum operating temperature of both the VZ-6000 and P40 (i.e., 258.15 K).

### C. Meteorological conditions and accumulation observed during Mass2Ant field campaigns

At the HAM site, three precipitation events were observed during the Mass2Ant 2018/19 field campaign [4]. The first event started by the end of Dec 29 and lasted until Jan 1, and was accompanied by high wind speed, exceeding  $10$  m s<sup>-1</sup>. On Jan 3, a second event was observed with snowfall and calm wind conditions [4]. From TLS data, these two events resulted in mostly accumulation in the scanned area [4]. On the contrary, we noticed patches with both net erosion and net accumulation as a result of the third high wind speed precipitation event that started on Jan 9. Moreover, the calculation of surface height increase from TLS data resulted in a 5 cm accumulation during the third precipitation event, averaged over the area [4]. Interestingly, this was found to be slightly above the first accumulation pattern (4 cm) and slightly below the accumulation that occurred between Dec 27 and Jan 4 (7.7 cm). Additionally, the SnowMicroPen (SMP) measurements show that the accumulation that occurred between Dec 27 and Jan 2 has a higher density compared to the accumulation in the period Jan 4 – Jan 11 (see Figures 7 and 8 in Wever et al. [4]). Also, relatively lower densities were observed in the period Dec 27 – Jan 4. These observations suggest that already existing low-density, snow layers were eroded by strong winds and are redeposited as high-density snow [4].

Similarly, two high wind speed precipitation events were observed during the Mass2Ant 2021/22 field campaign at the LIR site: a) the first event began at the end of Dec 27 and continued until early Dec 29, and b) the second event occurred between Jan 1 and Jan 2. These events were accompanied by wind speeds exceeding  $10$  m s<sup>-1</sup>. In the period Dec 25 – Jan 5, we observe a net accumulation of 7.3 cm computed



from TLS (see appendix, Fig. A.1). The net accumulation is calculated in similar way as that of the HAM site, i.e. averaged over the area. The observations during the field campaign period suggest the surface and accumulation conditions at the LIR site resemble that of the HAM site. Although the SMP measurements were not acquired at the LIR site, we use the inferences made at the HAM site as a reliable source for the LIR site.

#### D. Sentinel-1 SAR observations

The variability in radar return signal (or total backscatter) at the HAM and LIR sites is assessed using active microwave observations obtained by SAR onboard the Copernicus Sentinel-1 satellite constellation. In this study, we utilize the Level-1 GRD product of Sentinel-1 Extra Wide (EW) swath mode SAR images, featuring a spatial resolution of 40 m, and an incidence angle ranging from  $18^\circ$  to  $40^\circ$ . For the HAM and LIR site, we selected Sentinel-1 images between Dec 15 and Jan 15, for the 2018-19 and 2021-22 period, respectively, to coincide with the time of field measurements. Moreover, to examine the long-term changes, all the Sentinel-1 images in the period 2017-2023 are collected for both locations.

Pre-processing of the Sentinel-1 GRD data was done on the Google Earth Engine (GEE) platform, to which thermal noise removal, radiometric calibration, terrain correction using ASTER DEM is applied. First, we filtered the Level-1 GRD Sentinel-1 data (dB scale) using metadata attributes (i.e., bands: HH, HV, and incidence angle, orbits: ascending and descending, instrument mode: Extra Wide (EW) swath), temporal range, and the spatial bounds (i.e., the region of interest at HAM and LIR sites). Second, a masking operation was applied (i.e.,  $\sigma_{HV}^0 \leq \sigma_{HH}^0$ ) given the monostatic antenna configuration of Sentinel-1. Finally, the masked backscatter intensity values were converted to a linear scale.

#### E. Regional climate and firn models

In order to understand the changes in surface density, snowdrift erosion and wind-driven snow deposition processes at long time scales, we use output data from regional climate and firn models. The regional atmospheric climate model (RACMO2) [3] is a product of the Royal Netherlands Meteorology Institute (KNMI) and combines the High Resolution Limited Area Model (HIRLAM) numerical weather prediction model with the European Centre for Medium-Range Weather Forecasts Integrated Forecast System (IFS) physics [3]. Here, we employ the latest version, RACMO2.3p2, for Antarctica that includes a multilayer snow model and a bulk snowdrift model, forced by ERA5 reanalysis data every 3 hours from 1979-2022, which has been extensively validated over Antarctica [3]. In the absence of continuous roughness measurements for prolonged periods, we use the data of monthly averaged snowdrift erosion and snowfall variables at 27 km resolution for the period between 2016 and 2022 at the HAM and LIR site [26]. These variables are chosen as they represent the erosion/deposition (analogous to surface roughness), and accumulation conditions, respectively.

IMAU Firn Densification Model (IMAU-FDM) is a semi-empirical 1D model that simulates the transient evolution of a vertical firn column subject to firn and SMB processes [27]. We use the latest version, IMAU-FDM v1.2A, which is forced at its upper boundary by three-hourly fields of instantaneous surface temperature, 10-m wind speed, snowfall, sublimation, snowdrift erosion, snowmelt, and rainfall from RACMO2.3p2 [27]. The horizontal resolution of IMAU-FDM is determined by the resolution of RACMO2 (i.e., 27 km), whereas the temporal resolution is 10 days. For our analysis, we calculate the average density of upper 10 cm for the period 2016 – 2022, representing the variability in the snow surface density at the study sites.

### III. METHODS

#### A. Quantification of roughness from TLS data

Surface roughness can be quantified from two parameters: Root Mean Square height ( $RMS_h$ ) and Autocorrelation length ( $L_{auto}$ ), representing vertical and horizontal roughness components, respectively [22].  $RMS_h$  is the standard deviation of surface height variations, while  $L_{auto}$  measures the lag distance at which the value of the autocorrelation function of profile surface heights reaches  $e^{-1/2} \sim 0.606$  [22], [28]. To evaluate the horizontal component of roughness, we employ a 2D power spectrum analysis of topographical information derived from the in-situ TLS data [29]. This analysis utilizes the power spectral density (PSD) to decompose the surface into contributions from different spatial frequencies, providing an assessment of roughness and the lateral distribution of height variations [29]. By applying Fourier transformations, we compute the 2D PSD [29], [30]. The resulting PSD is then radially averaged to simplify computational complexity and characterize roughness by spatial frequency and angular averaging [31]. From the radially averaged PSD, we derive the autocorrelation function (ACF) through the inverse Fourier transform, allowing us to quantify spatial correlation and determine the  $L_{auto}$ .

For the HAM site, we calculated  $L_{auto}$  and  $RMS_h$  over  $1 \times 1 m^2$  patches at a spatial resolution of 1 mm, corresponding to the location of SMP measurements [4]. A total of 42 patches are used for Dec 27, Jan 2, and Jan 4, and 26 patches for Jan 11. All the patches are separated by  $\sim 90$  cm regular spacing. This is done in order to make reliable inferences on roughness analysis in combination with accumulation and surface density calculations from Wever et al. [4]. Since no SMP measurements were acquired at the LIR site, we calculated  $L_{auto}$  and  $RMS_h$  over a  $15 \times 15 m^2$  area from the scanned field to capture variations in roughness on 25 Dec 2021 and 5 Jan 2022. Further, dividing this larger area into 225 patches of  $1 \times 1 m^2$  allows for comparability with the HAM site. Using MATLAB, we compute the PSD and ACF for the sampled patches at different temporal instances during the measurement period and then,  $L_{auto}$  and  $RMS_h$  are calculated for each sampled patch.

## B. Scattering descriptors from Sentinel-1 GRD data

We use the pre-processed GRD data to compute the ratio of cross-pol (HV) to co-pol (HH) backscatter intensity, denoted as  $q_r$ , and defined in linear scale (equation 1).

$$q_r = \sigma_{HV}^0 / \sigma_{HH}^0; \quad 0 \leq q_r \leq 1 \quad (1)$$

Note that for the snow surface and a monostatic antenna configuration (similar to Sentinel-1), the cross-pol channel is usually less than the co-pol channel [32], [33], hence we assume  $\sigma_{HV} \leq \sigma_{HH}$ . Using  $q_r$ , we calculate  $\theta_c$  which describes the type of the scattering as per Bhogapurapu et al. [16]:

$$\tan \theta_c = \frac{(1 - q_r)^2}{1 + q_r^2 - q_r}; \quad 0^\circ \leq \theta_c \leq 45^\circ \quad (2)$$

The scattering-type parameter, denoted as  $\theta_c$ , serves as an indicator of dominant scattering scenarios. Based on Bhogapurapu et al. [16], when  $\theta_c = 45^\circ$ , a pure scattering scenario arises primarily from rough surface features, detectable at the radar wavelength. On the contrary,  $\theta_c = 0^\circ$  suggests a complex scattering scenario, mainly because of the dense and complex geometry of the canopy that makes the scattering increasingly unpredictable [16], due to the mixture of different types of scattering mechanisms (as highlighted in [34]).

We also derive the polarimetric scattering entropy (or pseudo-scattering entropy in dual-pol case),  $H_c$ , that quantifies the randomness or disorder in the polarization responses of the target [16]:

$$H_c = - \sum_{i=1}^2 p_i \log_2 p_i; \quad 0 \leq H_c \leq 1 \quad (3)$$

Here,  $p_1$  and  $p_2$  are pseudo probability measures given by  $1/(1+q_r)$  and  $q_r/(1+q_r)$ , respectively. A low  $H_c$  corresponds to a more ordered and uniform scattering behavior, wherein a single scattering (or isotropic scattering) is expected. A high  $H_c$  value indicates a more complex and diverse scattering environment with a random mixture of scattering mechanisms having equal probability of occurrence and, thus, a depolarizing target.

Both  $H_c$  and  $\theta_c$  parameters offer comprehensive insights into the target's scattering characteristics [16]. For instance, low entropy in pure scattering means single surface scattering due to more uniform roughness scales compared to the high entropy case, wherein pure scattering would mean multiple scattering at the surface caused by multi-scale rough surface features. Thus, the scattering-type parameter ( $\theta_c$ ) helps identify the dominant scattering mechanism, thereby providing a foundation for understanding the primary physical processes at play [16]. The entropy parameter complements this information by assessing the overall complexity and variability of the scattering behavior (i.e., whether single scattering is present or more than one scattering mechanisms co-exist). Bhogapurapu et al. [16] describe an unsupervised clustering framework where the  $H_c/\theta_c$  plane is divided into six discrete clusters, from a low entropy pure scattering to a high entropy complex scattering scenario. The curve is determined from

the relationship of  $H_c$  and  $\theta_c$  in the 2D clustering plane (Fig. 2(a)). For crop growth assessment, we see the potential of scattering parameters,  $H_c$  and  $\theta_c$ , in providing complementary information about the separation between pure scattering and volume scattering [16]. However, with discrete clusters, it is hard to quantify the dominant scattering from total backscatter. To avoid a subjective discretization of different clusters, we introduce a continuous angular variable,  $\alpha_{scat}$ :

$$\alpha_{scat} = \tan^{-1} \frac{\theta_c/45}{H_c}; \quad 0^\circ \leq \alpha_{scat} \leq 90^\circ \quad (4)$$

Before calculation,  $\theta_c$  is scaled to a 0–1 range by dividing it by  $45^\circ$ , thereby making it comparable to the range of  $H_c$ . We note that in the context of ice sheets, complex scattering can be treated interchangeably as a high entropy volume scattering scenario. This is because internal snow layering plays a predominant role in shaping the scattering response of the snowpack and, thus, contributing to volume scattering. More importantly, the occurrence of helix scattering, oriented dipole scattering, and compound dipole scattering is negligible, which forms a basis for complex scattering scenarios [34]. We thus use  $\alpha_{scat}$  to represent a complete scenario from the occurrence of volume scattering (i.e.,  $\alpha_{scat} = 0^\circ$ ,  $H_c = 1$ ,  $\theta_c = 0^\circ$ ) to pure scattering (i.e.,  $\alpha_{scat} = 90^\circ$ ,  $H_c = 0$ ,  $\theta_c = 45^\circ$ ).

The scattering indicator,  $\alpha_{scat}$ , is derived from  $H_c$  and  $\theta_c$ , which are in turn a function of  $q_r$  (Equation 4). Although the relationship between the two parameters exhibits some correlation (Figure 5 in [16]), the physical interpretations for targets differ significantly due to their fundamental formulations [16]. Bhogapurapu et al. [16] utilized a relation for the scattering of a polarized wave to express  $H_c$  in terms of the number of scattering events,  $n$ . This calculation is consistent with the derivation of Shannon entropy [35], [36]. With the increase in the number of scattering events, high order scattering (i.e., when  $n > 3$ ) saturates the  $H_c$  at  $\sim 0.7$ . In such scenario, the scattering is found to originate potentially from randomly oriented cylindrical scatterers [16]. On the other hand, a similar relationship is observed between the order of scattering and  $\theta_c$  [16], [13]. In this regard, we can approximately translate these physical interpretations to  $\alpha_{scat}$ , as it uses both the scattering-type and entropy information, thereby providing a comprehensive quantitative understanding of the dominant scattering mechanism.

With both Sentinel-1A and Sentinel-1B in operation, the revisit time for any point is considered to be approximately 6 days. However, the ground coverage is often more frequent over high latitudes, such as Antarctica, due to the geometry of their orbits. This means multiple orbits having different incidence angles, ranging from  $20^\circ$  to  $40^\circ$ , provide different perspective of the same location, thereby influencing the scattering characteristics and interpretation of Sentinel-1 signal. In Figure 2(b), we observe a strong relationship between incidence angle and  $\alpha_{scat}$ , with low values (or a tendency towards volume scattering) associated with low incidence angles and high incidence angles increase the tendency toward pure scattering. The normalization method applied to  $\alpha_{scat}$  values for the entire period (2017/2023) considers this variability, ensuring that the interpretation remains robust across different

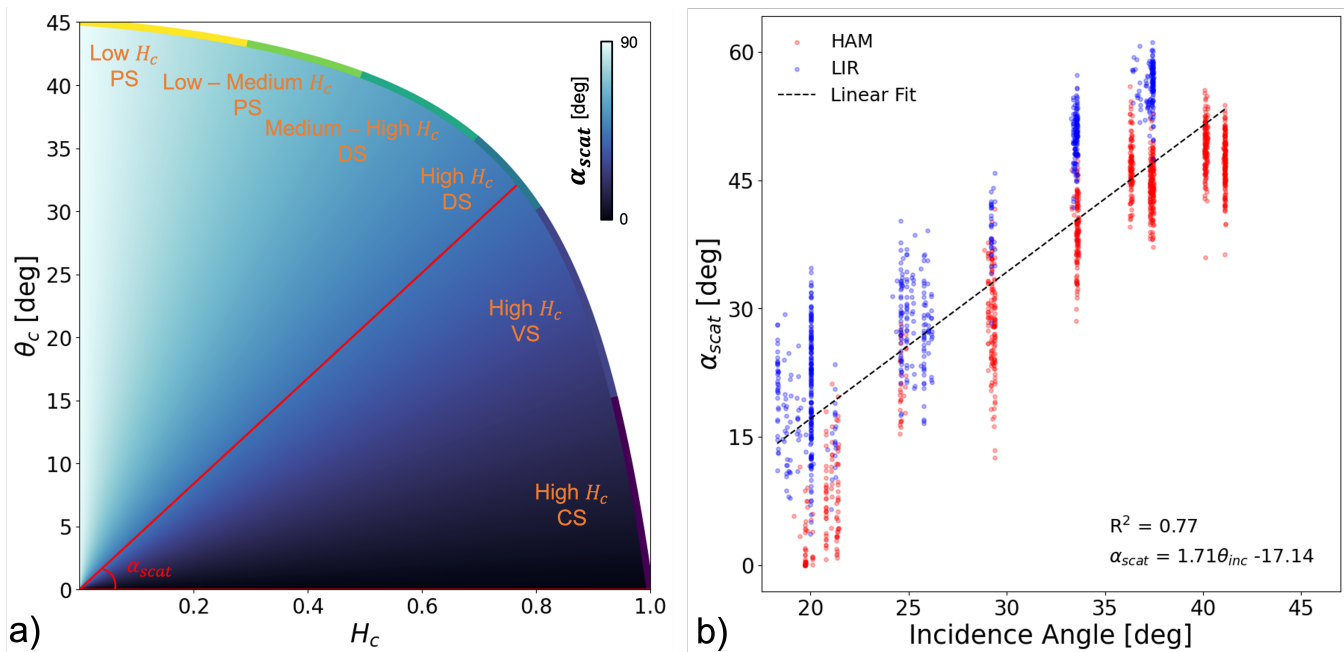


Fig. 2. a) 2D clustering plane ( $H_c/\theta_c$ ), with different scattering zones represented in orange color (adapted from Bhogapurapu et al. [16]). PS stands for Pure Scattering, DS stands for Distributed Scattering, VS stands for Volume Scattering, and CS stands for Complex Scattering [16]. Blue-white color space in the background represents the continuous transition of  $\alpha_{scat}$  with low and high values as a tendency to VS and PS, respectively. b) Incidence angle normalization using linear regression between  $\alpha_{scat}$  and incidence angle at the HAM and LIR site. The entire range of incidence angle in Sentinel-1 EW mode ( $18.9^\circ$  to  $47^\circ$ ) is depicted in the X-axis.

orbits. For this, we first consider a circular buffer of radius between 0 m and 1 km at a step of 200 m from the HAM and LIR station positions. Different buffer radii are mainly used to consider a broader area around the study sites and to make sure at least five orbits cover the region, thereby enhancing the incidence angle variability. We then average the  $\alpha_{scat}$  values derived from each buffer and plot them as a function of the incidence angle. Figure 2(b) depicts a linear fit with an  $R^2$  value of 0.77 between the incidence angle and the averaged  $\alpha_{scat}$  at the HAM and LIR sites. Ultimately, we use the residuals of linear regression,  $\alpha_{scat,\varepsilon}$ , to effectively explore the variability in dominant scattering mechanisms caused by changes in surface conditions. Analyzing the residuals enables us to focus on the variation that is not explained by incidence angle, thereby providing a more homogeneous understanding of the causes of scattering variability.

### C. Evaluation of Sentinel-1 $\alpha_{scat}$

In-situ measurements, such as roughness, surface density, and accumulation [4], are used to evaluate the  $\alpha_{scat}$  observations at the field scale. The focus is on examining changes in  $\alpha_{scat,\varepsilon}$  and roughness during designated periods between scan days. First, we calculate the ratio of vertical ( $L_{auto}$ ) to horizontal ( $RMS_h$ ) component for each sampled patch at different temporal instances in the HAM and LIR sites respectively. This ratio,  $L_{auto}/RMS_h$ , captures the roughness condition: high when the surface is smooth and low for a rough surface. Second, we systematically explore the temporal dynamics by considering all possible pairwise combinations of the scan days. Moreover, for every period, the change in

roughness ratio, averaged over the site, and the change in  $\alpha_{scat,\varepsilon}$  are calculated. We then compare the respective changes in every period throughout the entire field campaign to ensure the robustness of  $\alpha_{scat}$ , as we now utilize all the observations after incidence angle correction. Third, upper 10 cm snow density and accumulation rates [4] are linked to the observed change in  $\alpha_{scat,\varepsilon}$ .

For evaluating the long-term changes in  $\alpha_{scat,\varepsilon}$ , we analyze snow surface variables from RACMO2.3p2 and IMAU-FDM. The snowdrift erosion and snowfall variables are visualized at the temporal resolution of one month [26]. We derived monthly snow density in the uppermost 10 cm of the firm layer from IMAU-FDM to match with the RACMO2.3p2 products (i.e., one month). For more details on the accuracy of regional climate and firm models in simulating the snow surface conditions, we refer to [1], [3], [27]. To be consistent with the temporal resolution of snow surface variables, one-month moving average of  $\alpha_{scat,\varepsilon}$  is also considered.

## IV. RESULTS

### A. Surface roughness

Fig. 3 shows the evolution of  $RMS_h$  and  $L_{auto}$  for all sampled patches at the HAM and LIR sites discussed in Section III-A. The box plots express the spatial variability in roughness conditions. This variability is found to change over time both in magnitude, as well as in spread. Following accumulation and snow erosion patterns (as in figure 2 of Wever et al. [4]), we observe a gradual decrease in  $RMS_h$  (i.e., a smoothing effect) between Dec 27 and Jan 4 at the HAM site. However, the changes in  $L_{auto}$  are variable during

these accumulation phases: a decrease of 4.51 cm after the first high-wind speed accumulation pattern and an increase of 2.15 cm after the second, low-wind speed accumulation event, resulting in a net decrease of 2.37 cm in the period Dec 27 – Jan 4 (Fig. 3(b)).

Based on in-situ measurements, we observe almost similar accumulation amounts (4 cm and 3.7 cm) and similar higher temperatures (between 270 K and 273 K, from Figure 4 in Wever et al. [4]) for the periods Dec 27 – Jan 2 and Jan 2 – Jan 4 respectively. This suggests the primary differentiating factor driving the changes in  $RMS_h$  and  $L_{auto}$  between the two periods is the wind speed. Strong winds can impact the density of the snow when there is saltation [37], contributing to compaction in the snowpack. This results in the newly deposited snow having higher density in the form of crusts, while the density of the snow that was not mobilized remains more or less constant. In the absence of saltation, the density variations can also be caused by higher temperatures. When temperatures rise, snow grains may begin to melt slightly, leading to a process called sintering [10]. During this process, the grains bond together, which can increase the surface density of the snowpack. A similar observation was made in the field, wherein high-density layers were identified as discontinuous melt-freeze crusts and also captured by the SMP profile in the period Dec 27 – Jan 2 characterized by strong winds (see section II-C). Moreover, the wind-driven compaction tends to smooth out irregularities in the surface, reducing the vertical height, and hence, lower  $RMS_h$ . On the other hand, the force of the wind can also redistribute the snow particles horizontally. While this redistribution may not always necessarily lead to visible patterns of erosion, it contributes to a less uniform snow surface at shorter scales, resulting in a decrease in  $L_{auto}$ . Between Jan 2 and Jan 4, we witness snowfall under calm wind condition. The newly added snow resulted in a further decrease of  $RMS_h$  and increased the spatial wavelength of the surface ( $L_{auto}$ ), as there were no wind-induced alterations present.

In the period Jan 4 – Jan 11, a positive change of 0.15 cm in  $RMS_h$  is observed with a negative change of 2.16 cm in  $L_{auto}$  (Fig. 3), suggesting an increase in surface roughness. We attribute these changes to the presence of spatially variable erosion patterns even though there is a net accumulation of 5 cm. In the field, we noticed erodible snow near the surface. This indicates strong winds erode the short-lived low-density snow layers and re-deposits with higher density [4].

At the LIR site, we see a rapid transformation of the surface from very rough on 25 Dec 2021 (0.9 cm mean  $RMS_h$ ) to very smooth on 5 Jan 2022 (0.14 cm mean  $RMS_h$ ). This is also marked by an increase in  $L_{auto}$  of 3.7 cm. The smoothening effect is due to the high accumulation of 7.3 cm, as observed during the fieldwork in the period Dec 25 – Jan 5. Furthermore, the changes in roughness at the LIR site are found to be more pronounced than the HAM site. Overall, when accumulation dominates erosion, we witness longer  $L_{auto}$  with reduced  $RMS_h$  and, hence, a decrease in surface roughness. On the other hand, local erosion increases the roughness despite a net accumulation in the area, wherein

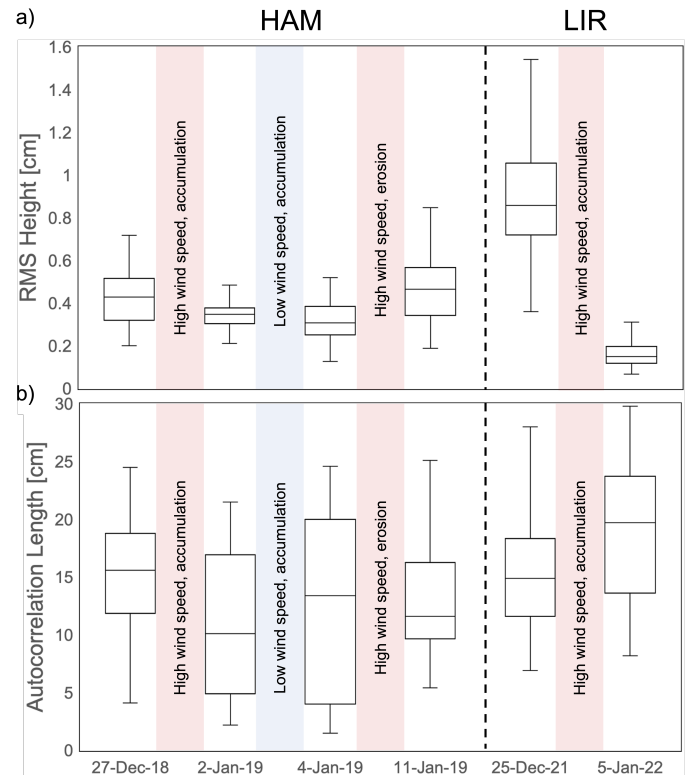


Fig. 3. Temporal variability of surface roughness at the HAM and LIR sites, represented by box plots. a)  $RMS_h$  and b)  $L_{auto}$  are derived from the TLS data acquired during field campaigns. Wind speed and accumulation/erosion conditions are also described (from Wever et al. [4])

the variations in  $RMS_h$  are more important.

### B. Sentinel-1 $\alpha_{scat,\epsilon}$ observations during Mass2Ant field campaigns

Fig. 4 illustrates the  $\alpha_{scat,\epsilon}$  from Sentinel-1 observations for the field campaign period. An increase in  $\alpha_{scat,\epsilon}$  indicates a tendency towards pure scattering, whereas a decrease is associated with a shift towards a volume scattering medium. There are no  $\alpha_{scat,\epsilon}$  values for certain scan days: i.e., Jan 2 and 4 for the HAM site and Dec 25 for the LIR site. We thus use the values from Jan 1 and 5 for the HAM site and Dec 24 at the LIR site, i.e., with a maximum difference of one day. This substitution is justified by the field observation that surface conditions during the selected days closely resemble those of the scan days, ensuring that our inferences remain unaffected. At the HAM site, we first see a decrease in  $\alpha_{scat,\epsilon}$  from Dec 27 to Jan 5 from  $-1.01^\circ$  to  $-12.18^\circ$ . This suggests a greater tendency towards volume scattering. The in-situ measurements showed higher snow accumulation of 7.7 cm in the period Dec 27 – Jan 5.

In contrast, the increasing trend that follows between Jan 5 to Jan 11 indicates a growing importance of pure scattering over volume scattering in the Sentinel-1 signal. Even though this period suggests a net accumulation, clear spatially variable erosion and deposition patterns cause complexity in the scattering behavior. Our interpretation is that initially, increasing wind speeds with only low precipitation amounts mostly

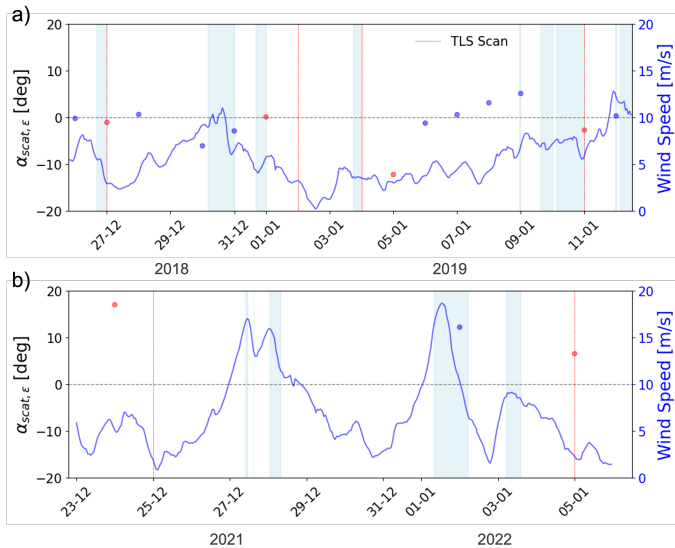


Fig. 4. Temporal variability of  $\alpha_{scat,\varepsilon}$  for the field campaign period at: a) HAM and b) LIR site. The light blue color in background is the period when precipitation occurs. Wind speed and precipitation are from the ERA-5 hourly dataset. TLS scan days are represented by a red line. Red dots are the  $\alpha_{scat,\varepsilon}$  values considered closest to field measurements, whereas blue dots represent the usual timeseries.

caused erosion and, associated with the erosion, an increase in pure scattering. The increased precipitation between Jan 9 – Jan 11 resulted in a net accumulation in the area, albeit in a variable pattern as indicated by the scans (Figure 2 in Wever et al. [4]). Yet, the net accumulation caused an associated decrease in  $\alpha_{scat,\varepsilon}$  values from  $5.15^\circ$  to  $-2.67^\circ$  in this period.

Although there are only three  $\alpha_{scat,\varepsilon}$  values at the LIR site corresponding to the field campaign period, one of them coincides with the scan days in the field. Fig. 4(b) shows a decline of  $\alpha_{scat,\varepsilon}$  (and thus, affinity towards volume scattering) in the period Dec 24 – Jan 5 with high accumulation. Moreover, the LIR site exhibits a rougher surface compared to the HAM site, with only positive  $\alpha_{scat,\varepsilon}$ , and higher  $RMS_h$  values (Fig. 3(a)), compared to the HAM site. In this regard, we see consistent behavior about the variations in  $\alpha_{scat,\varepsilon}$  due to changes in surface conditions both at HAM and LIR sites.

### C. Evaluation of $\alpha_{scat,\varepsilon}$ from in-situ measurements

In Fig. 5, we observe a relationship between  $\alpha_{scat,\varepsilon}$  and roughness ratio ( $L_{auto}/RMS_h$ ) where the change is calculated for each specified period at the HAM site. There is a very strong correlation between the change in roughness ratio and the change in  $\alpha_{scat,\varepsilon}$  ( $R^2 = 0.92$ , p-value = 0.002). A negative change in roughness ratio indicates that the surface is relatively rougher in that specific period, whereas a positive change is associated with smoother surfaces. We recall here that positive and negative changes in  $\alpha_{scat,\varepsilon}$  represent a tendency towards pure scattering and volume scattering, respectively.

The periods characterized by a positive change in roughness ratio (i.e., Dec 27 – Jan 4 and Jan 2 – Jan 4) correspond to a negative change in  $\alpha_{scat,\varepsilon}$ . A similar, yet more pronounced effect is observed at the LIR site. Here, the change in

roughness ratio between Dec 25 and Jan 5 is notably high (i.e., 96.86), accompanied by a significantly negative change in the  $\alpha_{scat,\varepsilon}$  value (i.e.,  $-10.46^\circ$ ). This indicates a strong tendency to volume scattering as roughness decreases due to higher accumulation rates. At the same time, low accumulation densities can also lead to increased volume scattering. Such a relationship was observed during the period Jan 2 – Jan 4 at the HAM site, where a much lower density of  $<200 \text{ kg m}^{-3}$  was recorded [4], showing the most negative change in  $\alpha_{scat,\varepsilon}$ .

On the contrary, a negative change in roughness ratio contributes to a positive change in  $\alpha_{scat,\varepsilon}$  (i.e., during the periods Dec 27 – Jan 2, Dec 27 – Jan 11, Jan 2 – Jan 11, and Jan 4 – Jan 11). We postulate that the dominant pure scattering mechanism is strongly influenced by the degree of surface roughness; thus, we anticipate a rougher surface to be a major source of pure scattering. Similar observations are also made in the work of Bhogapurapu et al. [16], where they found that the dominant variations in surface roughness contribute to the pure scattering mechanism. However, during the period Dec 27 – Jan 2, the surface is found to be relatively smooth yet there is a very slight positive change in  $\alpha_{scat,\varepsilon}$ . This can be explained by higher surface density from the accumulation pattern ( $\sim 350 \text{ kg m}^{-3}$ ) observed in the SMP profile [4], which resulted in a decreased tendency towards (expected) volume scattering behavior. Moreover, we also notice the behavior in increasing trend of  $\alpha_{scat,\varepsilon}$  in the period Dec 30 – Jan 1 despite accumulation (Fig. 4). On the other hand, although the accumulation in the period Jan 4 – Jan 11 (5 cm) is greater than that in Dec 27 – Jan 2 (4 cm), we observe that the change in  $\alpha_{scat,\varepsilon}$  is most positive, while the roughness ratio is most negative. Our analysis highlights that both surface density and roughness, influenced by erosion patterns, play crucial roles in determining pure scattering. However, the impact of these factors is further modulated by accumulation rates.

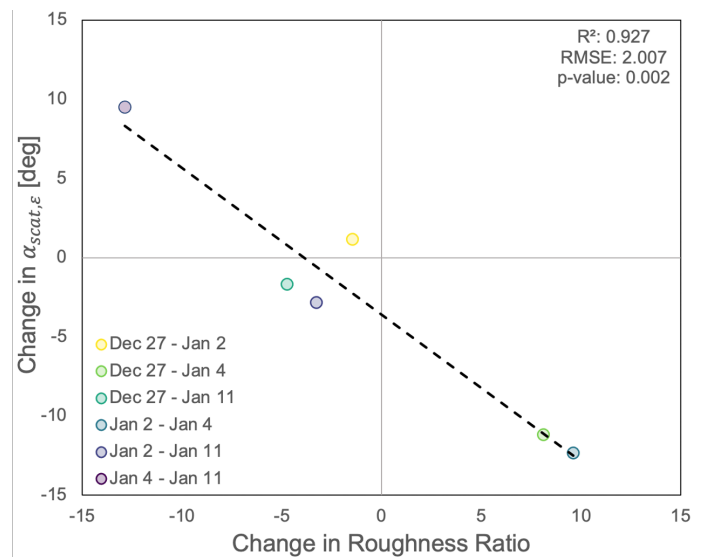


Fig. 5. Evaluation between change in  $\alpha_{scat,\varepsilon}$ , and roughness ratio for the HAM site.  $R^2$  is the coefficient of determination, RMSE is the root mean squared error in degree, and p-value shows the statistical significance of the analysis.



### D. Assessing the long-term changes in $\alpha_{scat,\varepsilon}$

Fig. 6 shows the long-term (2017/2023) timeseries of  $\alpha_{scat,\varepsilon}$ , smoothed with a one-month moving average, along with snow surface variables such as snowdrift erosion and snowfall simulated from RACMO2.3p2 and upper 10 cm density from IMAU-FDM. In the snowdrift erosion variable, positive values are associated with erosion, whereas negative values occur when there is wind-driven snow deposition [38]. At the HAM and LIR sites, there is a large temporal variability in both the snow properties and  $\alpha_{scat,\varepsilon}$ , and hence the dominant scattering mechanism, at seasonal to inter-annual time scales.

At the HAM site, we see an overall decrease of  $\alpha_{scat,\varepsilon}$  (from positive to negative) in the period 2017/2022, suggesting a gradual shift in the dominant scattering towards volume scattering (Fig. 6(a) and (b)). Moreover, we also notice a seasonal variability: an increasing tendency to volume scattering especially during winters, whereas the pure scattering mechanism remains dominant in summers. Furthermore, in the period 2022/2023, the  $\alpha_{scat,\varepsilon}$  values tend to recover, i.e., a slight increase after declining in the period 2017/2022.

In an attempt to understand the causes of the variability in  $\alpha_{scat,\varepsilon}$ , we examine the links between near-surface density and the dominant scattering. Looking at the summer periods, we see a rapid increase in density, which is typically accompanied by a seasonal maximum in the  $\alpha_{scat,\varepsilon}$  time series, indicating the increased tendency to pure scattering. The spike in surface density from  $\sim 400 \text{ kg m}^{-3}$  to  $\sim 650 \text{ kg m}^{-3}$  can be attributed to melt-related events, which could result in the formation of a high-density melt-freeze crust. Melt can further enhance surface roughness due to channeling and snow-albedo feedback, consequently increasing scattering from near-surface layers. Such crusts were also observed in the field at the HAM site in the period Dec 27 – Jan 2. It is important to note that due to resolution, the elevation of the RACMO2 grid point (i.e., 166 m for the HAM site and 194 m for the LIR site) is lower than the top of the ice rises where the actual field sites are located. This may mean that the effect of melt on density is higher in the simulations than in the field locations.

In years with pronounced density jumps (summers of 2017/2018 and 2019/2020),  $\alpha_{scat,\varepsilon}$  is found to increase more strongly than in years with limited density changes during summer. Additionally, deposition events (i.e., negative snowdrift values) are observed after the  $\alpha_{scat,\varepsilon}$  reaches the peak. These events add fresh snow to the surface, thereby decreasing the upper 10 cm density (also in Figure 6(a)) and increasing the tendency towards volume scattering. This is indicated by a decrease in  $\alpha_{scat,\varepsilon}$  values after the summer peak. Interestingly, the transition is variable, i.e., steeper in the summers of 2017/2018, 2018/2019, and 2019/2020 whereas it appears to be more gradual thereafter. These differences can be attributed to the intensity and duration of the deposition event. In the summers of 2017/2018 throughout 2019/2020, we observed relatively stronger deposition events lasting for a few months (represented by the wider and darker blue lines). However, from 2021 onward, a lower intensity of deposition events is depicted, leading to a gradual transition. In the

period 2022/2023, we observe positive values of snowdrift with almost no deposition. Such a scenario could indicate a tendency to pure scattering potentially caused by increased roughness (as observed in the period Jan 4 – Jan 11 in the field) and explain the recovery of  $\alpha_{scat,\varepsilon}$  values after a continuous decline until 2022.

Fig. 6(c) and (d) show that the variations in  $\alpha_{scat,\varepsilon}$  values at the LIR site show more complex behavior. As for HAM, we notice an increase in  $\alpha_{scat,\varepsilon}$  following rapid, melt-induced density changes in the summers of 2017/2018 and 2019/2020, followed by a decrease associated with snowdrift deposition and accumulation events, leading to more volume scattering. However, in the summer of 2018/2019, at the LIR site, the increase in  $\alpha_{scat,\varepsilon}$  cannot solely be explained by a near-surface density change, which shows a relatively small increase in this period. We note that the accumulation rates in the winter months (May – Sep) of 2019 were anomalously low ( $78.29 \text{ kg m}^{-2}$ ) and coincided with extended periods of snowdrift erosion. This could additionally contribute to an increased tendency towards pure scattering. On the contrary, during the period 2020/2021, a strong deposition event followed by higher accumulation rates ( $153.95 \text{ kg m}^{-2}$ ) in winter results in the drop of  $\alpha_{scat,\varepsilon}$ . Moreover, we observe an increase in  $\alpha_{scat,\varepsilon}$  after the summer of 2020/2021 compared to the period 2018/2021, mainly due to positive values of snowdrift (indicating strong erosion). Interestingly, even though the winter of 2021 experiences the highest accumulation ( $200.5 \text{ kg m}^{-2}$ ), snowdrift erosion remains a dominant source of pure scattering. This can also be clearly seen while comparing the  $\alpha_{scat,\varepsilon}$  time series in Fig. 6(a) and (c), wherein mostly positive values of snowdrift makes the LIR site a better pure scattering medium compared to the HAM site. We further notice that the total accumulation in the period 2017/2023 at the LIR site ( $\sim 2050 \text{ kg m}^{-2}$ ) is greater than that of the HAM site ( $\sim 1325 \text{ kg m}^{-2}$ ), which supports the inferences made from the field-scale analysis, i.e., strong erosion patterns result in an increase in  $\alpha_{scat,\varepsilon}$  despite net accumulation.

## V. DISCUSSION

Our analysis highlights the role of snow surface processes such as accumulation and snowdrift erosion in influencing the Sentinel-1  $\alpha_{scat,\varepsilon}$ . The addition of low-density snow layers during precipitation events results in a greater tendency to volume scattering, similar to the observations made by Lievens et al. [11]. Our findings align with the recent tower-mounted C-band radar experiments of alpine snowpacks, which show that volume scattering predominates during dry snow accumulation [39]. However, we demonstrate that strong winds can erode the low-density surface layers [4], thereby increasing the roughness and the tendency towards pure scattering despite net accumulation. This suggests that there is a complex relationship between accumulation rates and surface roughness, akin to Studinger et al. [40]'s explanation. Such a scenario makes it challenging to explain the causes behind the changes in  $\alpha_{scat,\varepsilon}$  based on a single snow surface variable, where the interplay between different variables needs to be considered.

At seasonal time scales, surface density and  $\alpha_{scat,\varepsilon}$  at the HAM site exhibit a consistent pattern, in line with field



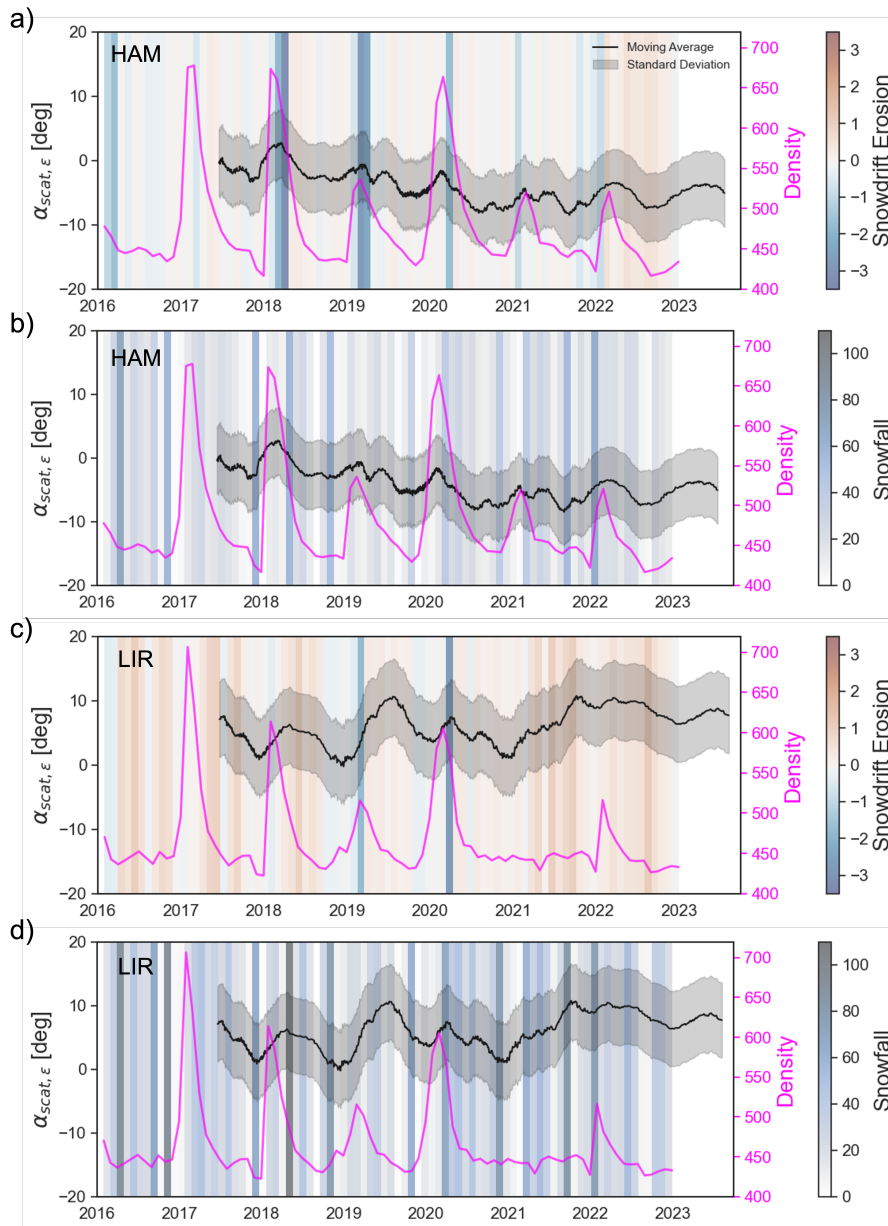


Fig. 6. Long-term evolution of  $\alpha_{scat,\epsilon}$ , upper 10 cm surface density from IMAU-FDM ( $\text{kg m}^{-3}$ ), snowdrift erosion, and snowfall from RACMO2.3p2 ( $\text{kg m}^{-2}$ ). The shaded region denotes 1 standard deviation of  $\alpha_{scat,\epsilon}$  from the mean.

measurements. This indicates that surface density, along with roughness, contributes to the increase in  $\alpha_{scat,\epsilon}$  despite net accumulation. Similar inferences are also found in Brangers et al. [39] stating that the presence of melt-freeze crusts (and thus, high density surface layers) have a strong effect on the observed backscatter even when the snow depth remains constant. A contrasting behavior is, however, observed at the LIR site. One potential explanation could be the higher accumulation rates at the LIR site, which may suppress the effect of surface density given their role in enhancing the volume scattering. Moving forward, further work needs to establish the combined effect of roughness, surface density, and accumulation rates on the dominance of pure scattering from  $\alpha_{scat,\epsilon}$ .

It remains unclear whether the relationship between  $\alpha_{scat,\epsilon}$  and snow surface processes identified in this study can be generalized beyond the specific area examined here. Both the study sites fall in an accumulation zone characterized by consistent katabatic winds [18]. Other sites, associated with high melting, may behave differently. Moreover, a point-by-point linear regression approach for incidence angle normalization may not always yield robust results due to the variability in correlation strength across different locations. This variability could pose challenges for consistent and accurate normalization, potentially leading to weak positive, weak negative, or even no correlation in some areas. While the current approach works effectively for regional-scale analysis, its application at an Antarctic-wide scale may necessitate a more robust and

generalized approach.

One of the main advantages of our study sites is the unique repeated in-situ data of roughness, which, however, is not readily available elsewhere. We thus highlight the importance of our study as a proof-of-concept to quantify the dominant scattering mechanism from near-surface layers (pure scattering) and internal snow layers (volume scattering). This provides new opportunities to understand the sensitivity of the C-band radar signal to the seasonal patterns of snow accumulation and erosion, similar to Brangers et al. [39]. Our study further demonstrates the potential of Sentinel-1 SAR: a) to capture the complex interaction of accumulation, erosion, and surface density in a drifting snow environment, and b) as a proxy to changes in snow surface properties. At the same time, more repeated in-situ measurements of roughness and surface density from multiple locations in Antarctica are required to calibrate our proposed parameter  $\alpha_{scat,\varepsilon}$ . However, obtaining down-scaled climate model parameters then also becomes important, to remove the uncertainty from grid point representativeness for the field locations. This could for example be obtained with higher model spatial resolutions than currently used in RACMO2, or using statistical downscaling methods [41] as a viable alternative.

While the current study focuses on Antarctic snow surfaces, the method could also be applied to mountain glaciers (e.g., in the Himalayan and Alps regions) and ice caps with certain considerations. These regions may experience different climatic conditions, such as higher temperatures and variable precipitation patterns, which can affect snow density and surface roughness differently. For instance, higher temperatures may lead to more frequent melt-refreeze cycles, altering the snow microstructure and potentially affecting the scattering mechanisms observed by Sentinel-1 [42]. Additionally, the influence of topography on wind patterns, subsequent snow deposition and erosion processes, and incidence angle normalization needs to be considered, as these factors can vary significantly between polar and mountainous regions. Adaptations in the methodology may involve incorporating local climate data and topographical influences to accurately capture the scattering behavior in these environments.

In addition to expanding field data, we emphasize the importance of utilizing radiative transfer (RT) models to comprehend the sensitivity of  $\alpha_{scat,\varepsilon}$  to surface properties and snow microstructure variations. Currently, the state-of-the-art models, such as Snow Microwave Radiative Transfer (SMRT) [43], and Advanced Integral Equation Model (AIEM) [44], do not include the multiple scattering events caused because of surface roughness, thereby restricting the model capability to simulate the cross-pol backscatter (HV), which is an important component in  $\alpha_{scat,\varepsilon}$ . Moreover, the RT simulations can provide further evidence for the importance of  $\alpha_{scat,\varepsilon}$  over  $q_r$ , as it is virtually impossible to demonstrate this empirically. We thus encourage future modeling efforts to assess the current challenges in understanding the  $\alpha_{scat,\varepsilon}$  variations.

We note that the spatial scales of surface roughness, the snow structure, and the wavelength of the sensor are significantly different. This suggests that the sensor's wavelength

(i.e., C-band) could not be ideally matched with either surface roughness or snow structure, posing challenges in accurately capturing changes in surface snow processes. Different radar frequencies offer varying penetration depths, which could lead to a better separation of changes induced by roughness and internal snow layers in  $\alpha_{scat,\varepsilon}$ . However, integrating multi-frequency SAR data into the analysis pipeline presents practical challenges. One major challenge is the development of sophisticated algorithms capable of effectively combining data from different frequencies, which requires addressing differences in spatial resolution, temporal alignment, and signal-to-noise ratios. Another challenge is the need for extensive sensor calibration to ensure consistency across datasets, as variations in calibration and acquisition geometries can introduce discrepancies in the data. Additionally, handling large volumes of data from multiple frequencies necessitates significant computational resources and storage capacity. Despite these challenges, the use of multi-frequency observations holds great potential for advancing our understanding of snow surface dynamics and improving the accuracy of snow process monitoring.

Looking ahead, future SAR missions such as ESA ROSE-L and NISAR, which operate in L/S-band, offer promising opportunities to enhance our understanding of snow surface processes. These missions will provide quad-pol data, which can yield additional information on backscatter mechanisms influenced by varying surface conditions. For instance, the cross-polarized channels ( $HV$  and  $VH$ ) are particularly sensitive to volume scattering from internal snow layers, while the co-polarized channels ( $HH$  and  $VV$ ) provide insights into surface roughness and density variations [33]. By integrating these diverse polarization measurements, it becomes possible to better isolate and understand the contributions of different scattering mechanisms to the observed backscatter signal. Incorporating data from advanced missions could significantly improve the methodological framework of  $\alpha_{scat,\varepsilon}$  as a parameter for monitoring snow surface properties by disentangling the complex interplay between surface roughness, accumulation, and density.

## VI. CONCLUSION

In this study, we focused on the relationship between surface processes and the dominant scattering mechanism from Sentinel-1 in East Antarctica. We introduced a new parameter derived from scattering-type and entropy descriptors based on [16] and normalized for incidence angle effects,  $\alpha_{scat,\varepsilon}$ . This parameter quantifies the continuous scattering response from near-surface layers (i.e., pure scattering) and from internal snow layers (i.e., volume scattering). The changes in  $\alpha_{scat,\varepsilon}$  are evaluated from the repeated in-situ surface measurements acquired during Mass2Ant field campaigns, which include roughness and accumulation derived from terrestrial laser scanner (TLS), and surface densities from Wever et al. [4]. At the field-scale, our analysis shows a strong correlation between roughness and  $\alpha_{scat,\varepsilon}$ . During periods associated with erosion, the vertical component of roughness ( $RMSh$ ) is found to be more important than the horizontal component ( $L_{auto}$ ) in

changing the scattering response. This is also marked by an increase in  $\alpha_{scat,\varepsilon}$  value (or tendency towards pure scattering). In contrast, accumulation patterns lead to surface smoothing with dominant scattering from internal snow layers. From long-term changes in  $\alpha_{scat,\varepsilon}$ , high surface densities are found to be related to an increase in pure scattering. A similar correspondence is also observed in the field. However, increasing (decreasing) accumulation rates potentially contribute to suppressing (enhancing) the effect of surface density on dominant scattering. We need more field data, especially the repeated measurements, from multiple locations and radiative transfer model simulations to quantify the combined effect of roughness, surface density, and accumulation rates on dominant scattering mechanisms from Sentinel-1. This will lead to a better separation between pure and volume scattering, thereby providing an effective framework to assess the connection between SMB processes and dominant scattering mechanisms in Sentinel-1 observations.

#### APPENDIX

For the field site at LIR, the difference between TLS scans on 25 Dec 2021 and 5 Jan 2022 is shown in Fig. A.1. We see that the surface is mostly dominated by a positive change in snow depth and that the erosion and accumulation patterns are spatially variable.

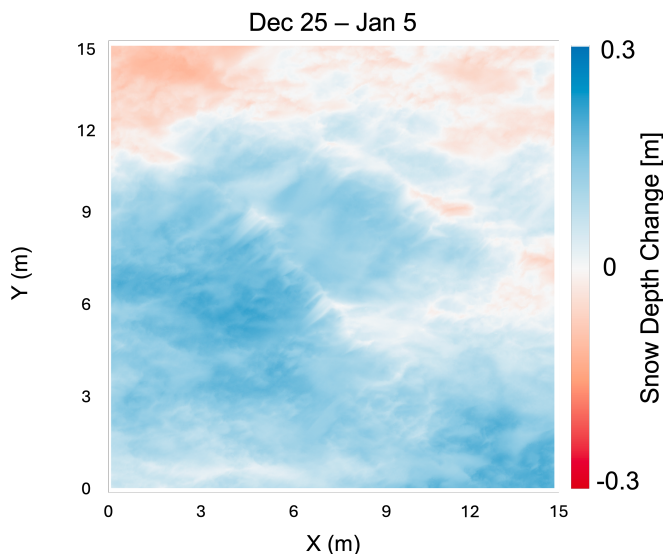


Fig. A.1. Snow depth change between Dec 25 and Jan 5, calculated from laser scans obtained on both days in the 2021–22 field season on the LIR site ( $15 \times 15 \text{ m}^2$ ).

#### ACKNOWLEDGMENT

We acknowledge the International Polar Foundation for supporting the logistics during the field campaigns at HAM and LIR sites. The 2018/19 and 2021/22 field campaigns are part of Mass2Ant project funded by the Netherlands Organisation for Scientific Research (grant no. AL-WPT.2016.4), the Belgian Federal Science Policy Office (grant no. BR/165/A2:Mass2Ant), and the National Aeronautics and

Space Administration (grant no. 80NSSC18K0201). Additionally, we sincerely acknowledge Prof. Roland Klees from TU Delft for his significant help and support in the frequency domain analysis of TLS data to derive the roughness information. We also thank the reviewers for their helpful and thorough comments.

#### REFERENCES

- [1] J. T. M. Lenaerts, B. Medley, M. R. van den Broeke, and B. Wouters, "Observing and Modeling Ice Sheet Surface Mass Balance," *Reviews of geophysics (Washington, D.C. : 1985)*, vol. 57(2), pp. 376–420, 6 2019.
- [2] C. Amory, C. Buizert, S. Buzzard, E. Case, N. Clerx, R. Culberg, R. T. Datta, R. Dey, R. Drews, D. Dunmire, C. Eayrs, N. Hansen, A. Humbert, A. Kaitheri, K. Keegan, P. Kuipers Munneke, J. T. M. Lenaerts, S. Lhermitte, D. Mair, I. McDowell, J. Mejia, C. R. Meyer, E. Morris, D. Moser, F. M. Oraschewski, E. Pearce, S. de Roda Husman, N.-J. Schlegel, T. Schultz, S. B. Simonsen, C. M. Stevens, E. R. Thomas, M. Thompson-Munson, N. Wever, B. Wouters, and T. F. S. team, "Firm on ice sheets," *Nature Reviews Earth & Environment*, Jan 2024. [Online]. Available: <https://doi.org/10.1038/s43017-023-00507-9>
- [3] J. M. van Wessem, W. Jan Van De Berg, B. P. Y. Noël, E. van Meijgaard, C. Amory, G. Birnbaum, C. L. Jakobs, K. Krüger, J. T. M. Lenaerts, S. Lhermitte, S. R. M. Ligtenberg, B. Medley, C. H. Reijmer, K. Van Tricht, L. D. Trusel, L. H. van Ulft, B. Wouters, J. Wuite, and M. R. Van Den Broeke, "Modelling the climate and surface mass balance of polar ice sheets using RACMO2 : Part 2: Antarctica (1979-2016)," Apr. 2018.
- [4] N. Wever, E. Keenan, C. Amory, M. Lehning, A. Sigmund, H. Huwald, and J. T. M. Lenaerts, "Observations and simulations of new snow density in the drifting snow-dominated environment of Antarctica," *Journal of Glaciology*, pp. 1–18, 12 2022.
- [5] T. Nagler, H. Rott, E. Ripper, G. Bippus, and M. Hetzenecker, "Advancements for snowmelt monitoring by means of sentinel-1 sar," *Remote Sensing*, vol. 8, no. 4, p. 348, 2016.
- [6] C. Gabarró, N. Hughes, J. Wilkinson, L. Bertino, A. Bracher, T. Diehl, W. Dierking, V. Gonzalez-Gambau, T. Lavergne, T. Madurell, E. Malnes, and P. M. Wagner, "Improving satellite-based monitoring of the polar regions: Identification of research and capacity gaps," *Frontiers in Remote Sensing*, vol. 4, p. 952091, 2023.
- [7] R. Torres, P. Snoeij, D. Geudtner, D. Bibby, M. Davidson, E. Attema, P. Potin, B. Rommen, N. Floury, M. Brown, I. N. Traver, P. Deghaye, B. Duesmann, B. Rosich, N. Miranda, C. Bruno, M. L'Abbate, R. Croci, A. Pietropaolo, M. Huchler, and F. Rostan, "GMES Sentinel-1 mission," *Remote Sensing of Environment*, vol. 120, pp. 9–24, 5 2012.
- [8] T. Nagler, H. Rott, M. Hetzenecker, J. Wuite, and P. Potin, "The Sentinel-1 Mission: New Opportunities for Ice Sheet Observations," *Remote Sensing*, vol. 7, no. 7, pp. 9371–9389, 7 2015.
- [9] F. T. Ulaby and D. G. Long, *Microwave Radar and Radiometric Remote Sensing*. Ann Arbor, Michigan: The University of Michigan Press, 2014.
- [10] C. G. Sommer, N. Wever, C. Fierz, and M. Lehning, "Investigation of a wind-packing event in queen maud land, antarctica," *The Cryosphere*, vol. 12, no. 9, pp. 2923–2939, 2018. [Online]. Available: <https://tc.copernicus.org/articles/12/2923/2018/>
- [11] H. Lievens, M. Demuzere, H.-P. Marshall, R. H. Reichle, L. Brucker, I. Brangers, P. de Rosnay, M. Dumont, M. Giroto, W. W. Immerzeel, T. Jonas, E. J. Kim, I. Koch, C. Marty, T. Saloranta, J. Schöber, and G. J. M. De Lannoy, "Snow depth variability in the Northern Hemisphere mountains observed from space," *Nature Communications*, vol. 10, no. 1, p. 4629, Oct. 2019.
- [12] C. Mätzler, E. Schanda, R. Hofer, and W. Good, "Microwave signatures of the natural snow cover at weissfluhjoch," in *Microwave Remote Sensing of Snowpack Properties*, ser. NASA Conference Publication 2153, no. 19810010996. Fort Collins, Colorado: NASA Goddard Space Flight Center, Scientific and Technical Information Office, May 1980, pp. 203–223.
- [13] S. Cloude, "The dual polarization entropy/alpha decomposition: A pilsar case study," *Science and Applications of SAR Polarimetry and Polarimetric Interferometry*, vol. 644, p. 2, 2007.
- [14] S. Cloude and E. Pottier, "A review of target decomposition theorems in radar polarimetry," *IEEE Transactions on Geoscience and Remote Sensing*, vol. 34, no. 2, pp. 498–518, 1996.

- [15] T. L. Ainsworth, J. Kelly, and J.-S. Lee, "Polarimetric analysis of dual polarimetric sar imagery," *Proceedings of the European Conference on Synthetic Aperture Radar, EUSAR*, vol. 7, pp. 1–4, 2008.
- [16] N. Bhogapurapu, S. Dey, A. Bhattacharya, D. Mandal, J. M. Lopez-Sanchez, H. McNairn, C. López-Martínez, and Y. S. Rao, "Dual-polarimetric descriptors from Sentinel-1 GRD SAR data for crop growth assessment," *ISPRS Journal of Photogrammetry and Remote Sensing*, vol. 178, pp. 20–35, 8 2021.
- [17] K. Matsuoka, R. C. A. Hindmarsh, G. Moholdt, M. J. Bentley, H. D. Pritchard, J. Brown, H. Conway, R. Drews, G. Durand, D. Goldberg, T. Hattermann, J. Kingslake, J. T. Lenaerts, C. Martín, R. Mulvaney, K. W. Nicholls, F. Pattyn, N. Ross, T. Scambos, and P. L. Whitehouse, "Antarctic ice rises and rumpled: Their properties and significance for ice-sheet dynamics and evolution," *Earth-Science Reviews*, vol. 150, pp. 724–745, 11 2015.
- [18] T. Kausch, S. Lhermitte, J. T. M. Lenaerts, N. Wever, M. Inoue, F. Pattyn, S. Sun, S. Wauthy, J.-L. Tison, and W. J. van de Berg, "Impact of coastal East Antarctic ice rises on surface mass balance: insights from observations and modeling," *The Cryosphere*, vol. 14, no. 10, pp. 3367–3380, 10 2020.
- [19] J. T. M. Lenaerts, J. Brown, M. R. van Den Broeke, K. Matsuoka, R. Drews, D. Callens, M. Philippe, I. V. Gorodetskaya, E. van Meijgaard, C. H. Reijmer, F. Pattyn, and N. P. M. van Lipzig, "High variability of climate and surface mass balance induced by antarctic ice rises," *Journal of Glaciology*, vol. 60, no. 224, p. 1101–1110, 2014.
- [20] L. Dong, N. Baghdadi, and R. Ludwig, "Validation of the AIEM Through Correlation Length Parameterization at Field Scale Using Radar Imagery in a Semi-Arid Environment," *IEEE Geoscience and Remote Sensing Letters*, vol. 10, no. 3, pp. 461–465, 5 2013.
- [21] N. Baghdadi, C. King, A. Chanzy, and J. P. Wigneron, "An empirical calibration of the integral equation model based on SAR data, soil moisture and surface roughness measurement over bare soils," *International Journal of Remote Sensing*, vol. 23, no. 20, pp. 4325–4340, 1 2002.
- [22] A. K. Fung and K. S. Chen, *Microwave Scattering and Emission Models for Users*, 1st ed. Norwood, MA: Artech House Publishers, 2010.
- [23] Leica Cyclone, "Leica Cyclone: Technical Specifications," Leica Geosystems AG, 9435 Heerbrugg, Switzerland, Tech. Rep., 2017.
- [24] A. Prokop, M. Schirmer, M. Rub, M. Lehning, and M. Stocker, "A comparison of measurement methods: terrestrial laser scanning, tachymetry and snow probing for the determination of the spatial snow-depth distribution on slopes," *Annals of Glaciology*, vol. 49, pp. 210–216, 9 2008.
- [25] G. Walsh, "Leica ScanStation: Details that Matter," Leica Geosystems AG, 9435 Heerbrugg, Switzerland, Tech. Rep., 2020.
- [26] J. M. van Wessem, W. J. van de Berg, and M. R. van den Broeke, "Data set: Monthly averaged RACMO2.3p2 variables (1979-2022); Antarctica," Apr. 2023. [Online]. Available: <https://doi.org/10.5281/zenodo.7845736>
- [27] S. B. M. Veldhuijsen, W. J. van de Berg, M. Brils, P. Kuipers Munneke, and M. R. van den Broeke, "Characteristics of the 1979–2020 antarctic firn layer simulated with imau-fdm v1.2a," *The Cryosphere*, vol. 17, no. 4, pp. 1675–1696, 2023. [Online]. Available: <https://tc.copernicus.org/articles/17/1675/2023/>
- [28] R. Ménard, M. Deshaies-Jacques, and N. Gasset, "A comparison of correlation-length estimation methods for the objective analysis of surface pollutants at environment and climate change canada," *Journal of the Air & Waste Management Association*, vol. 66, no. 9, pp. 874–895, 2016, pMID: 27104336. [Online]. Available: <https://doi.org/10.1080/10962247.2016.1177620>
- [29] T. D. B. Jacobs, T. Junge, and L. Pastewka, "Quantitative characterization of surface topography using spectral analysis," *Surface Topography: Metrology and Properties*, vol. 5, no. 1, p. 013001, 1 2017.
- [30] F. M. Mwema, E. T. Akinlabi, and O. P. Oladijo, "The Use of Power Spectrum Density for Surface Characterization of Thin Films," in *Photoenergy and Thin Film Materials*. Beverly, Massachusetts: Scrivener Publishing, Wiley Global, 2019.
- [31] Y. Gong, S. T. Mixture, P. Gao, and N. P. Mellott, "Surface Roughness Measurements Using Power Spectrum Density Analysis with Enhanced Spatial Correlation Length," *The Journal of Physical Chemistry C*, vol. 120, no. 39, pp. 22358–22364, 10 2016.
- [32] I. Hajnsek, G. Parrella, A. Marino, T. Eltoft, M. Necsoiu, L. Eriksson, and M. Watanabe, *Cryosphere Applications*. Cham: Springer International Publishing, 2021, pp. 179–213. [Online]. Available: [https://doi.org/10.1007/978-3-030-56504-6\\_4](https://doi.org/10.1007/978-3-030-56504-6_4)
- [33] S. Cloude, *Polarisation: applications in remote sensing*. OUP Oxford, 2009.
- [34] G. Singh and Y. Yamaguchi, "Model-based six-component scattering matrix power decomposition," *IEEE Transactions on Geoscience and Remote Sensing*, vol. 56, no. 10, pp. 5687–5704, 2018.
- [35] D. Bicout and C. Brosseau, "Multiply scattered waves through a spatially random medium: entropy production and depolarization," *Journal de Physique I*, vol. 2, no. 11, pp. 2047–2063, 1992.
- [36] C. Brosseau, "Polarization transfer and entropy transformation," *Optik (Stuttgart)*, vol. 88, no. 3, pp. 109–117, 1991.
- [37] C. G. SOMMER, M. LEHNING, and C. FIERZ, "Wind tunnel experiments: saltation is necessary for wind-packing," *Journal of Glaciology*, vol. 63, no. 242, p. 950–958, 2017.
- [38] J. T. Lenaerts, M. R. Van Den Broeke, C. Sarchilli, and C. Agosta, "Impact of model resolution on simulated wind, drifting snow and surface mass balance in terre adélie, east antarctica," *Journal of Glaciology*, vol. 58, no. 211, p. 821–829, 2012.
- [39] I. Brangers, H.-P. Marshall, G. De Lannoy, D. Dumire, C. Matzler, and H. Lievens, "Tower-based c-band radar measurements of an alpine snowpack," *EGUsphere*, vol. 2023, pp. 1–25, 2023. [Online]. Available: <https://egusphere.copernicus.org/preprints/2023/egusphere-2023-2927/>
- [40] M. Studinger, B. C. Medley, K. M. Brunt, K. A. Casey, N. T. Kurtz, S. S. Manizade, T. A. Neumann, and T. B. Overly, "Temporal and spatial variability in surface roughness and accumulation rate around 88 s from repeat airborne geophysical surveys," *The Cryosphere*, vol. 14, no. 10, pp. 3287–3308, 2020. [Online]. Available: <https://tc.copernicus.org/articles/14/3287/2020/>
- [41] B. Noël, J. M. van Wessem, B. Wouters, L. Trusel, S. Lhermitte, and M. R. van den Broeke, "Higher antarctic ice sheet accumulation and surface melt rates revealed at 2 km resolution," *Nature Communications*, vol. 14, no. 1, p. 7949, Dec 2023. [Online]. Available: <https://doi.org/10.1038/s41467-023-43584-6>
- [42] H. Lievens, I. Brangers, H.-P. Marshall, T. Jonas, M. Olefs, and G. De Lannoy, "Sentinel-1 snow depth retrieval at sub-kilometer resolution over the european alps," *The Cryosphere*, vol. 16, no. 1, pp. 159–177, 2022. [Online]. Available: <https://tc.copernicus.org/articles/16/159/2022/>
- [43] G. Picard, M. Sandells, and H. Löwe, "SMRT: an active-passive microwave radiative transfer model for snow with multiple microstructure and scattering formulations (v1.0)," *Geoscientific Model Development*, vol. 11, no. 7, pp. 2763–2788, 7 2018.
- [44] T. D. Wu, K. S. Chen, S. Jiancheng, L. Hung-Wei, and A. K. Fung, "A Study of an AIEM Model for Bistatic Scattering From Randomly Rough Surfaces," *IEEE Transactions on Geoscience and Remote Sensing*, vol. 46, no. 9, pp. 2584–2598, 9 2008.

## BIOGRAPHY SECTION



**Shashwat Shukla** received his Masters degree in Geo-information Science and Earth Observation from University of Twente in 2019. He is currently pursuing his Ph.D. degree at the Delft University of Technology (TU Delft), researching Antarctic surface and subsurface processes using multi-source radar observations and radiative transfer models. His research interests include monitoring the physical properties at Earth and planetary surfaces from innovative remote sensing frameworks.



**Bert Wouters** received his Masters degree and PhD at the Faculty of Aerospace Engineering, after which he worked as a post-doc at KNMI (NL), the Universities of Boulder (USA) and Bristol, (UK) and the IMAU institute at Utrecht University (NL). He has been with the Faculty of Civil Engineering and Geosciences, Delft University of Technology (NL) since 2018. His research revolves around remote sensing of the climate, in particular of the cryosphere, and combining these observations with model data.





**Ghislain Picard** received the M.Sc. degree in remote sensing from the University of Paris VII, Paris, France, in 1997, and the Ph.D. degree from the Center d'Etudes Spatiale de la Biosphere (CESBIO), Toulouse, France, in 2002. In 2005, he joined the Institut des Géosciences de l'Environnement, Université Grenoble-Alpes, Grenoble, France, where he has been a Full Professor, since 2018. He is involved in the development of innovative instruments for the characterization of the snow-physical properties and of optical and microwave radiative transfer (RT)

models. His research interests include the Antarctic climate observed through the study of snow using a variety of remote sensing techniques and field experimentation.



**Nander Wever** received the Ph.D. degree in Environmental Engineering from the EPFL, Lausanne, Switzerland, in 2015. His PhD research was carried out at the WSL Institute for Snow and Avalanche Research SLF in Davos, Switzerland. Between 2017 and 2022, he worked at the University of Colorado, Boulder, Colorado, USA on modelling snow and firn processes in the polar regions, such as snow on sea ice, drifting snow, snow compaction and water percolation in firn. He is currently a research scientist at the WSL/SLF and MeteoSwiss in Zurich,

Switzerland. His current research focuses on modelling snow processes in stand-alone snow models and numerical weather prediction models, covering alpine snowpacks, snow on sea ice, and firn on ice sheets. During research expeditions to Antarctica and the Antarctic sea ice, he collected field measurements that helped to improve parameterizations in snow models and to understand the impact of drifting and blowing snow on snow redistribution and snow properties.



**Maaïke Izeboud** received the B.Sc. and M.Sc. degree in civil engineering from Delft University of Technology, Delft, The Netherlands in 2016 and 2019 respectively. She will defend her Ph.D. degree at Delft University of Technology in October 2024. Her research is focused on studying damage on the ice shelves of Antarctica using multi-source satellite imagery.



**Sophie de Roda Husman** obtained a B.Sc. degree and M.Sc. degrees in Civil Engineering from Delft University of Technology in 2017 and 2020, respectively. She is currently pursuing her Ph.D. degree at the TU Delft, researching Antarctic surface melt and hydrology using multi-source satellite imagery.



**Thore Kausch** received his B.Sc. degree in Physics of the earth system and his M.Sc. degrees Geophysics from the Christian Albrechts University in Kiel. From 2018 to 2022 he was a full time PhD candidate at the TU Delft, researching the surface mass balance of East Antarctica. Currently he is still writing on the Thesis of this PhD. Since 2022 he is employed as a software engineer for Bareways GmbH in Lübeck, Germany.



**Sanne Veldhuijsen** received the B.Sc. degree in 2018, in earth sciences and the M.Sc. degree in 2020, in hydrology from Utrecht University, Utrecht, the Netherlands, where she is currently working toward the Ph.D. degree with the Institute for Marine and Atmospheric Research Utrecht (IMAU), working on improved modeling of the current and future Antarctic firn layer for which she uses numerical and machine learning models.



**Christian Mätzler** was born in 1945 in Kreuzlingen, Switzerland. He studied physics at the University of Bern, with minors in mathematics and geography, M.Sc. in 1970, and Ph.D. in solar radio astronomy in 1974. After postdoctoral research at the NASA Goddard Space Flight Center, Greenbelt, MD, and at the Swiss Federal Institute of Technology (ETH), Zürich, Switzerland, he became Research Group Leader for terrestrial and atmospheric radiometry and remote sensing at the Institute of Applied Physics, University of Bern in 1978. There he received the habilitation in applied physics in 1986 and the title of a Titular Professor in 1992. He spent sabbaticals in 1996 at the Universities of Colorado and Washington and in 2004 at the Paris Observatory. After retirement in July 2010, he started as a consultant for Gamma Remote Sensing. His studies have concentrated on microwave (1–100 GHz) signatures for active and passive remote sensing of the atmosphere, snow, ice, soil, and vegetation, as well as on the development of methods for dielectric and propagation measurements for such media. He is Editor of a book on thermal microwave emission with applications in remote sensing. He is interested in physical processes acting at the earth surface and in the atmosphere.

received the habilitation in applied physics in 1986 and the title of a Titular Professor in 1992. He spent sabbaticals in 1996 at the Universities of Colorado and Washington and in 2004 at the Paris Observatory. After retirement in July 2010, he started as a consultant for Gamma Remote Sensing. His studies have concentrated on microwave (1–100 GHz) signatures for active and passive remote sensing of the atmosphere, snow, ice, soil, and vegetation, as well as on the development of methods for dielectric and propagation measurements for such media. He is Editor of a book on thermal microwave emission with applications in remote sensing. He is interested in physical processes acting at the earth surface and in the atmosphere.



**Stef Lhermitte** is a remote sensing scientist with specific interest in the use of multi-source remote sensing and land surface modelling to assess cryosphere, atmosphere and ecosystem dynamics. Since 2022 Stef Lhermitte is Associate Research Professor at KU Leuven (Belgium) which he combines with a position as Associate Professor at Delft University of Technology (Netherlands) since 2016. Before that, he obtained a PhD in bioscience engineering at KU Leuven in 2008 and did several international post-docs positions (CEAZA, KNMI,

KULeuven), where he worked on broad range of remote sensing technologies in a variety of applications ranging from cryospheric and atmospheric sciences to ecology and hydrology. Now he focuses on the development of innovative remote sensing methods for assessing land-atmosphere interactions in order to assess the effect of climate (change) on the cryosphere, ecosystem dynamics, the hydrological cycle, sea level rise, etc. and their feedbacks on (future) climate.